DICE/CASA/MIA

ELSEVIER

Astroparticle Physics 13 (2000) 137–150

Astroparticle Physics

www.elsevier.nl/locate/astropart

Elemental composition of cosmic rays near the knee by multiparameter measurements of air showers

S.P. Swordy [a], D.B. Kieda [b,*]

[a] *Enrico Fermi Institute and Department of Physics, University of Chicago, Chicago IL 60637, USA*
[b] *Department of Physics, University of Utah, Salt Lake City, UT 84112, USA*

Received 28 July 1999; accepted 17 September 1999

Abstract

The small change in the spectral slope of the overall intensity of cosmic rays near 1 PeV may be associated with the endpoint energy of supernova shock acceleration. A crucial test of this connection and other ideas of the origin of the spectral 'knee' is the reliable determination of the variation of elemental composition in this region. Recent measurements at the DICE/CASA/MIA air shower installation in Dugway, Utah, USA have provided several independent air shower parameters for each event. The derivation of elemental composition from a combination of Cherenkov size, depth of shower maximum in the atmosphere, muon size and electron size at ground level and the reliability of these results are discussed. There is no evidence from these data for a large change in the mean mass of cosmic rays across the 'knee'. These measurements show the cosmic rays are composed of $\sim 70\%$ protons and α particles near total energies of 10 PeV. © 2000 Elsevier Science B.V. All rights reserved.

1. Introduction

The slight steepening in the power law spectrum of the cosmic-ray flux near energies of $10^{15.5}$ eV has provoked a wide range of interpretations since its discovery in air shower size spectra nearly 40 years ago [1]. This spectral 'knee' remains an enigma, which together with the more recently discovered flattening (or 'ankle') near $10^{18.5}$ eV provide the only known features in the arriving cosmic-ray spectrum at high energy. The coincidence of the 'knee' with the maximum energies expected from diffusive shock acceleration in supernova remnants, has served to cement its value as a key region for further investigation in cosmic-ray research. The features which might better connect the change in overall spectral slope with expectations from shock acceleration lie in the details of the individual elemental spectra hidden within the overall cosmic-ray flux. The accurate determination of the elemental composition across the knee region, from $\sim 10^{14}$ to 10^{16} eV, is a crucial measurement yet to be made.

Recent observations of supernovae using TeV γ rays have not managed to detect [2] the signal expected from high-energy cosmic-ray collisions with local material if supernova remnants (SNR) are the sources of high-energy cosmic rays [3]. Although EGRET has reported GeV γ rays from some SNRs [4], it is still unclear if the signal is produced by locally intense cosmic rays [5]. Non-thermal x-ray emissions have been detected from two SNRs [6,7]

* Corresponding author.
E-mail address: kieda@krusty.physics.utah.edu (D.B. Kieda).

0927-6505/00/$ - see front matter © 2000 Elsevier Science B.V. All rights reserved.
PII: S0927-6505(99)00117-6

which have been interpreted as synchrotron emission from local electrons at energies up to ~ 100 TeV [8], but the source spectral slope inferred by these results seems inconsistent with the electron source spectrum derived from direct measurements. It remains the case that the most convincing argument for supernovae explosions producing the bulk of the cosmic rays arises from the staggering power required to maintain the population given the measured lifetime of particles within our Galaxy. A typical value for the power needed is $\sim 10^{40}$ erg/s (see, e.g., Schlickeiser [9]), based on a cosmic-ray residence time of $\sim 10^7$ years, a time-scale directly inferred from measurements of the surviving amount of the radioactive isotopes of Be^{10} [10] and Al^{26} [11] which are created by spallation reactions of cosmic rays on interstellar material.

2. Air shower detectors

While direct detection above the atmosphere is clearly the most desirable method for composition determination, the fluxes of particles in this energy range are so small that a detector large enough to collect a good statistical sample up to 10 PeV (1 PeV $= 10^{15}$ eV) has not yet been built. Indirect detection of cosmic rays, through measurements of air showers produced in the atmosphere, can easily supply sufficient collecting power but these methods generally have poor resolution for the properties of the originating cosmic-ray nucleus whose identity becomes clouded by the huge number of interactions in the air shower. Further, the reconstruction of the mass of the incoming nucleus from measurements of the shower distributions at ground level is subject to systematic errors introduced by reliance on shower modeling by numerical simulations.

To address these issues we have constructed and operated a new type of experiment designed specifically for cosmic-ray measurements near the knee. This Dual Imaging Cherenkov Experiment (DICE) is a ground-based air shower detector which is designed to have as little reliance as possible on the details of the air shower simulations and to have the capability of comparison with existing direct measurements at 0.1 PeV to provide an assessment of the overall systematic error. DICE operates at the site of the Chicago Air Shower Array (CASA) and the MIchigan Array (MIA) which are designed as an observatory for PeV γ rays. They can also be used to examine hadronic showers since they give measurements of electron size and muon size at ground level.

2.1. DICE description

Since the method of imaging hadronic showers in Cherenkov light is a relatively recent development, we provide some more detailed description of the DICE detectors and operation. The two DICE telescopes are located at the CASA-MIA site in Dugway, Utah (described in Borione et al. (1994) [12]). They each consist of a 2 m diameter f/1.16 spherical mirror with a focal plane detector of 256 close packed 40 mm hexagonal photomultipliers (PMTs) which provide $\sim 1^0$ pixels in an overall field of view $16^0 \times 13.5^0$ centered about the vertical. The telescopes are on fixed mounts separated by 100 m (see Boothby et al. [13,14]).

Cosmic-ray events within the field of view produce a focal plane image at the PMT cluster which corresponds to the direction and intensity of Cherenkov light coming from the air shower. When the direction of the air shower core and the distance of the shower axis from the telescopes are known, simple geometry can be used to reconstruct the amount of light received from each altitude of the shower. The amount of Cherenkov light produced is strongly correlated with the number of electrons in the shower and is used to estimate the electron size as a function of depth in the atmosphere from which the location of shower maximum can be determined. This procedure is essentially geometrical and is independent of numerical simulations except for calculations which determine the angular distribution of Cherenkov light around the shower axis.

2.2. CASA / MIA description

The CASA/MIA installation and operation is described in detail in Borione et al. 1994 [12]. In this present work, information from CASA-MIA is used to establish the event geometry and to directly measure the electron size and muon size at ground level. Since the event acceptance is constrained by the DICE aperture, only events within $\sim 10^0$ of the

enith are analyzed, making the atmospheric depth of he size measurements to be essentially the same for ll events at ~ 860 g/cm^2.

3. Measured parameters

For each air shower collected, a simple time oincidence is used to identify the same event in oth DICE clusters and CASA-MIA. Further requirements on the correlation of the DICE images with ach other and with the CASA-MIA event geometry re used to reduce the overall probability of event nismatches between the detectors to $\sim 10^{-5}$. The asic independent parameters measured for each hower are shown in Table 1.

The parameters for each shower are derived from hese measured values. The accuracy of the shower ore location derived by CASA is 1–3 m depending n the overall shower size. The measurement of the hower arrival direction is accurate to $\sim 0.4^0$ for arger showers with some degradation for lower energy events. These measurements and their errors are iscussed in detail in Borione et al. 1994 [12]. The lectron size from CASA is derived from a fit to the measured particle intensities to signals produced in an array of plastic scintillation counters using the NKG formulism [15,16]. The muon size is a fit to signals produced in buried scintillators using the function discussed by Greisen [15]. Further details of these fits are discussed in McKay [17].

3.1. Derived shower parameters

Some of the shower parameters used in this analysis correspond directly to measured values. The electron and muon sizes at ground level (N_e and N_μ) are

Table 1
Parameters measured for each event.

Description	Symbol used here	Source instrument
Shower direction and core location		CASA
Cherenkov size	Ch	DICE
Shower maximum	X_{max}	DICE
Electron size at ground	N_e	CASA
Muon size at ground	N_μ	MIA

those derived by CASA/MIA. The Cherenkov size at the two DICE detectors is obtained by summing the total amount of light detected at each photomultiplier tube (PMT) cluster. The location of shower maximum in the atmosphere (X_{max}) is determined by fitting the shape of the shower image in each of the DICE PMT clusters. The Cherenkov light from each height in the shower falls into a specific angular bin in the focal plane when the event geometry is known. By applying corrections for solid angle, the variation of light emission intensity with respect to the shower axis, and corrections for atmospheric absorption, a profile of electron size versus atmospheric depth is developed from the Cherenkov image. This is fit with a simple two parameter shower shape to find the location of shower maximum in each DICE telescope. An estimate for (X_{max}) is found for both DICE clusters, a crucial difference between DICE and detectors which fit the lateral distribution of Cherenkov light is that this estimate of (X_{max}) is based on simple geometry. It does not rely on the details of numerical simulations or have stringent linearity requirements of the detectors.

Previous work with DICE estimated the shower energy by a simple translation from the total amount of Cherenkov light in the image and the geometry of the shower [18]. In this present work a more accurate estimate of energy is derived from a combination of the amount of Cherenkov light and the X_{max} determination produced by each DICE telescope. This is desirable since the lateral distribution and intensity of Cherenkov light at a given total energy depends both on the primary particle mass, hence mean X_{max}, and the distance of the measurement from the shower core. A fit for the total shower energy and primary particle mass is made to the geometry, Cherenkov size (Ch) and X_{max} location in the two DICE telescopes. The form of the Cherenkov size function used in these fits is derived from the results of simulations using the program CORSIKA 4.50 with the VENUS interaction model [19]. The derived X_{max} fitting function has a constant shower elongation rate parameter and assumes simple superposition for providing primary particle mass dependence. The exact form of both of these fitting functions are given in Appendix A as Eqs. (A.1) and A.2.

Events collected by DICE in coincidence with CASA/MIA over a period from mid 1994 to early

1996 are subjected to the following selection cuts before fitting with Eqs. (A.1) and (A.2). (1) The core of the shower lies at a distance $100\,\mathrm{m} < r < 225$ m from both DICE telescopes. (2) The fits of the longitudinal development in both DICE telescopes have reduced $\chi^2 < 3$. (3) The X_{max} from each telescope agrees within 150 g/cm^2. (4) The arrival direction of the shower is within 6^0 of the vertical. The fits to the measured *Ch* and X_{max} from the two sites are made using the minimum χ^2 method. With these cuts the effective collection geometry is determined by the instrument Monte Carlo to be ~ 3300 m^2 sr, making the overall collecting power $\sim$ 125 000 m^2 sr days. Using the detailed calculated aperture and efficiency corrections derived from an instrument Monte Carlo discussed below the cosmic-ray energy spectrum can be constructed from the fit energies. This is shown as the filled circles in Fig. 1 together with previous determinations of the energy spectra in this region. The fluxes have been multiplied by $E^{2.75}$ to emphasize the change in slope across the knee region. These agree with the previously reported energy spectrum for DICE [18]. We believe this new analysis provides a better determination of fluxes because of the primary mass dependent fitting function used for each event. These new DICE data are given in tabular form in Appendix B. The 'knee' here is at an energy around 3 PeV.

The mean measured values of X_{max} as a function of energy is shown in Fig. 2. Here these values are

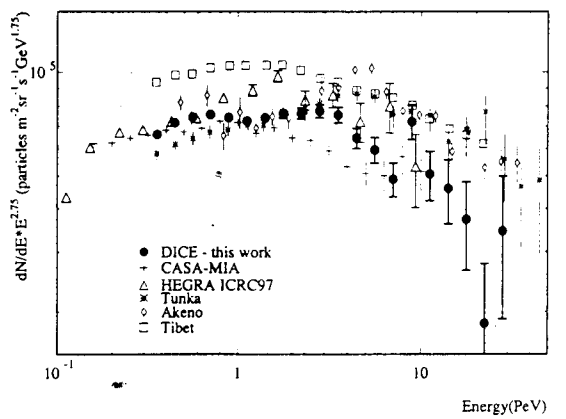

Fig. 1. Measurements of energy spectra near the 'knee' from this work (filled circles) compared with recent measurements from Tibet [23], CASA-MIA [24], HEGRA [20], Tunka [21], and Akeno [25].

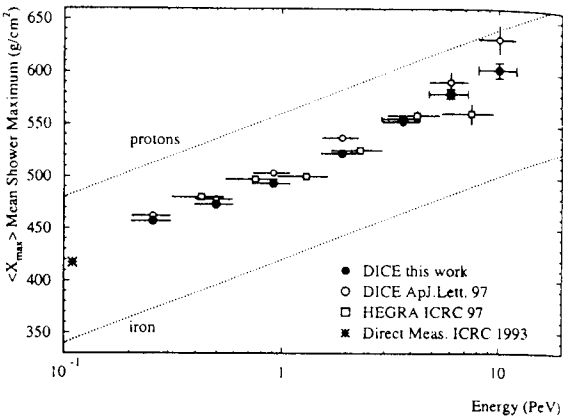

Fig. 2. Measurements of mean X_{max} versus energy.

compared with the previous DICE results [18] and those of the HEGRA experiment determination [20] which uses the distribution of Cherenkov light at ground level to estimate X_{max}. The star shows the expectation for the mean X_{max} based on a the direct composition measured near 100 TeV [22] using Eq. (A.2). The various measurements show general agreement, although there is a tendency for the DICE results to show a lighter composition at the highest energy. The present data are in statistical agreement with the previously published results of DICE, but they show somewhat less departure from constant composition at high energies. The dashed lines are for pure proton or pure iron composition given by Eq. (A.2). These results are tabulated in Appendix B.

3.2. Robustness of shower parameters

The determination of incident particle mass from air shower measurements have generally poor resolution. Consequently features such as elemental peaks, which can commonly be used in direct measurements of cosmic rays to test detector calibration, are absent. This makes systematic sources of error the largest obstacle which must be overcome in order to produce a reliable measurement. Any internal consistency checks which can be used on the data are valuable as a way to keep these problems to a minimum. The combination of DICE and CASA/MIA provides a unique combination of shower parameters which overdetermine the characteristics of each shower. The comparison of parameters from different detectors can be used to test the

reliability of results. This process is already possible within DICE since the separate measurements of X_{max} and *Ch* made with each cluster can be compared to test consistency. A more rigorous test is a comparison of the information derived from DICE with that from CASA/MIA.

The general profile of air showers produced by hadrons has been studied by several authors. These showers can be thought of as a succession of electromagnetic showers fed by a core of interacting hadrons. The fluctuations in shower maximum are produced both by the statistical nature of the shower development and the fluctuations in the first interaction point in the atmosphere. At atmospheric depths deeper than X_{max}, the shower size declines in a manner which is dominated by the atmospheric hadronic interaction length. If the size is measured at a depth relative to the location of X_{max} the fluctuations produced by variations in the initial interaction point are removed. We can perform a simple test on the data discussed here: Does the electron size at ground level measured by CASA fit with the shower energy and location of X_{max} produced by DICE? By using the average shower development function quoted by Gaisser [26] (given in Appendix A), we can compare the expected ground electron size with the CASA measurement.

Since showers at a given energy have values of X_{max} which fluctuate for the reasons outlined above, we can sample a range of potential electron sizes versus X_{max} for a specific primary energy range. This procedure can be used to verify the consistency of measurements and to test for systematic errors in the determination of X_{max}, E, and N_e as a function of energy. If at a ground level depth of X_0 we compare $N_e(X_0)/E$ with X_{max} for each event, we can test on average if these agree with Eq. (A.3) over a range of parameters. Fig. 3 shows how this test works for X_{max} and E determined from DICE and N_e from CASA. The four panels correspond to some of the energy bins used for Fig. 2. Each panel shows the average $\log10(N_e/E)$ plotted versus shower X_{max}. The function derived from the average air shower development (from Eq. (A.3)) is shown as a solid line. The good agreement between the measurements and the data for the lower energy data provide confidence that the location of X_{max} determined by DICE and the electron size at ground level are

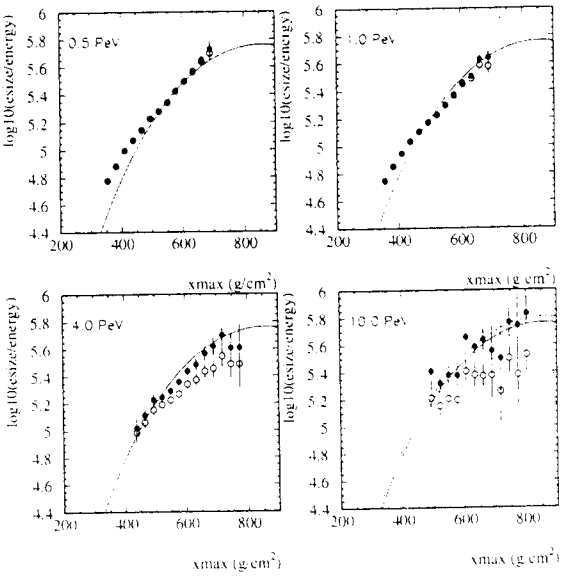

Fig. 3. Comparisons of expected electron size at ground with a shower model from Gaisser [26]. The open symbols represent raw electron sizes, the filled symbols are electron sizes corrected for saturation in a manner discussed in the text.

measured correctly. The version of the Gaisser function shown as the dashed curve in the lower right-hand panel of Fig. 3 shows the effect of scaling violation as discussed in Appendix A.3.

It is important to realize that not just the shower shape but the normalization of the shower size versus X_{max} is given by Eq. (A.3), there is no arbitrary vertical normalization of the curves shown in Fig. 3. These results therefore also provide confidence that the measurement of energy from DICE is reasonable, an error in energy would produce a systematic shift of the data in the vertical direction. For the higher energies there appears to be a small systematic shift, of the order of 10%, of the data to a region below the curve. This could be produced by a various effects; (i) the energy scale is overestimated at the higher energies, (ii) the electron size is underestimated for large electron sizes, (iii) the location of X_{max} is overestimated for high energies. This last possibility seems unlikely since the method used for the measurement of X_{max} is the same at both low and high energies and no similar systematic shift appears across all energies. For example the region for X_{max} near 700 g/cm^2 is sampled both by the 1 PeV and 10 PeV energy, at the lower energy the measure-

ments agree with the expected curve, at higher energies they do not. A systematic error in the determination of X_{max} for deep showers should produce a similar shift at both energies. The lack of a systematic shift across all energies also shows that errors in X_{max} produced by atmospheric scattering of Cherenkov light is minimal, since this would also only depend on the depth of maximum shower size. The first possibility, (i) mentioned above, also seems unlikely since there would be a large effect on the energy spectrum shown in Fig. 1. A shift in the energy scale measure of the required magnitude ($\sim$ 20%) would produce a significant increase in the apparent fluxes at the higher energies ($\sim 40\%$), which does not seem to be present in the data. We are left with the possibility that the electron size somehow 'saturates' slightly at the higher energies if we believe Eq. (A.3) is independent of energy. This is a possibility since CASA, primarily built for observations near 100TeV, was not designed to operate for air shower core density measurements at 10 PeV. The electron sizes at high energy are predominantly derived from counters on the perimeter of the core which have not saturated. We have developed a simple correction to the electron size for large values which apparently corrects the discrepancy shown in Fig. 3. This is given by

$$\log_{10} N_{ec} = \log_{10} N_e, \qquad \log_{10} N_e < 5.5,$$

$$\log_{10} N_{ec} = \log_{10} N_e \times \left(1 + (\log_{10} N_e - 5.5) \times 0.04\right),$$

$$\log_{10} N_e \geq 5.5,$$

where N_{ec} is the corrected electron size, N_e is the original size and E is the shower energy in PeV as described above. This increases the electron size by around $\sim 7\%$ near energies of 10 PeV. This simple parameterization provides a much better fit to the shower curves in Fig. 3 as shown by the filled symbols identified as 'saturation corrected data'. We use this corrected electron size through the rest of this paper. Importantly this change is not large, but illustrates the power of correlating apparently redundant measurements. These can be used to explore systematic problems with various measured quantities.

4. Mass determination

In this analysis we adopt a slightly different philosophy from previous work by using combinations of measured parameters to derive an incident particle mass, A, on a shower by shower basis. With the information presented above we form two estimates for the mass, one from the location of X_{max} and the fitted shower energy and another from the muon and electron sizes in combination with the fitted energy.

4.1. Mass functions

Although mass functions of arbitrary complexity can in principle be derived from analysis of numerical simulations, these are not always transparent as to the underlying physical processes which produce the sensitivity to mass from a particular combination of parameters. Here we adopt the approach of using a simple physical model to produce a mass function which is tested against simulations to determine the accuracy of this function over some range of energies. We first make some simple assumptions about the variation of shower parameters for singly charged particles with energy,

$$X_{max} = X_0 + X_m \times \log_{10}(E),$$

$$N_\mu = N_{\mu 0} \times E^\alpha,$$

where X_0, X_m, $N_{\mu 0}$, α, are constants and E is the energy in PeV. Typical values for the scaling constants are $X_m = 80$ g/cm^2 and $\alpha = 0.87$. We assume simple superposition to define how these will vary for heavier particles of mass A,

$$X_{max} = X_0 + X_m \times \log_{10}(E/A),$$

$$\mu_g = \log_{10}(A) + \alpha \times \log_{10}(E/A),$$

where $\mu_g = \log_{10}(N_\mu/N_{\mu 0})$ and the first of these equations is the same as (A.2). We can rearrange these to give an estimate for the mass A,

$$\log_{10}(A)_x = (X_0 - X_{max})/X_m + \log_{10}(E), \qquad (1)$$

$$\log_{10}(A)_g = \left(\mu_g - \alpha \times \log_{10}(E)\right)/(1-\alpha), \qquad (2)$$

where $\log_{10}(A)_x$ is the mass from the measurement of X_{max} and $\log_{10}(A)_g$ is the mass from the mea-

surement of muon size at ground level. At fixed energy, deeper showers (larger X_{max}) give a smaller mass and muon rich showers (larger μ_e) give a larger mass. Another feature of these mass estimate equations is that they have an opposite sign dependence on the shower energy. Hence errors in energy assignment produce opposing errors in the mass estimates. In principle these estimates can be used to make independent mass estimates from the same showers. Eq. (1) results from the location of the hadronic shower maximum and Eq. (2) arises from the energy of the pions decaying into muons in the shower. At the same total energy, proton showers have typically higher energy pions than iron showers so heavier nuclei produce more muons from pion decays in the shower development.

There is however another factor which effects the muon size at ground level. This is slightly dependent on X_{max} in a similar but much weaker fashion to the electron size dependency discussed above and shown in Fig. 3. Fluctuations in shower development produce larger muon sizes at ground level when X_{max} is larger for the same initial energy. Although this is not a large effect, the mass estimate described in Eq. (2) is sensitive to small fluctuations in μ_e because of the small value of $(1-\alpha)$ in the denominator. These fluctuations are strongly correlated with the electron size at ground level and their effect can be significantly reduced by introducing a correction term based on $e_e = \ln(N_e/N_{e0})$, the normalized electron size at ground level. The overall mass function derived from muon measurements using this correction is given by

$$\log_{10}(A)_e = \left(\mu_e - \alpha \times \log_{10}(E) - \delta(e_e)\right) / (1-\alpha), \quad (3)$$

where the correction $\delta(e_e)$ is applied to reduce fluctuations in muon size arising from variations in the shower development. This correction is discussed in detail in Appendix C.

4.2. Correlations of mass estimates

To investigate the consistency of these mass estimates we can look at the variations of one type of mass estimate versus the other. This is shown in Fig. 4 for some of the energy bins studied. The correlation between these estimates over a range of energies provides confidence that the estimates are roughly correct. This correlation has some small contribution from the common energy term in Eqs. (1) and (2), this is not large since a fluctuation in energy of 30% only produces a change in either mass function of ~ 0.1. The dominant contribution to this correlation is from the rapid variation of electron size measured at the ground with X_{max} depth as shown in Fig. 3. Although clearly μ_e plays a role, since there are more muons from showers produced by heavier primaries, the fluctuations of showers at some fixed primary energy and mass provide wide enough variations in X_{max} to make the electron size effect predominate. In some sense the correlations in Fig. 4 are a straightforward result of the relationships shown in Fig. 3.

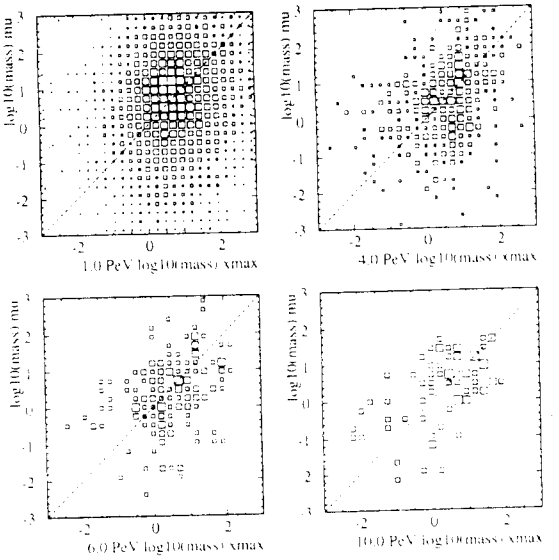

Fig. 4. Cross correlation plots of the mass determinations from X_{max} and the muon size for events in energy bins similar to Fig. 2. The size of each box is linearly proportional to the number of events, concentration of the events are expected along the dashed lines if the correlation is good. The mass functions are discussed in the text.

4.3. Comparison with simulations

To further test these distributions and methods for estimating mass we can compare these results with the expectations from simulations. These calculations

must take account of shower properties, detector properties, and the analysis cuts used. A simulation program was developed which uses the results of air showers produced by the CORSIKA 4.5 code as an input for the shower characteristics. The simulation effort was concentrated on the DICE measurements of X_{max}, all the details of the fluctuations in the quantities directly affecting these were included. The electron sizes and muon sizes at ground level are included but the fluctuations in these are parameterized in a simplified fashion to speed up the calculations. These simulated showers impact on the detector site at random locations and angles near the vertical in the simulation. The output of the simulation is a data file which can be subjected to exactly the same cuts and analysis procedures applied to the actual data. For the analysis discussed here the input primary mass composition used in the simulation is a constant 30% H, 30% He, 10% CNO, 10% NeMgSi, and 20% Fe. As discussed later, there is no evidence for significant variation in this composition across the range of energies in this work. The simulation is also generated with a spectral shape which approximates the variation in slope through the knee region. and includes details of the contributions from shower geometry, focal plane pixel size, etc. The simulation can also be used to determine the overall effective geometrical factor of the instrument. This was used in combination with the instrument livetime to calculate the normalization of the data in Fig. 1.

We can compare the shape of the X_{max} mass estimates from DICE with the predictions from the simulation. This provides a test of the overall consistency of the method used and can exclude certain extreme composition possibilities. The left-hand panel of Fig. 5 shows the r.m.s. value of $\log_{10}(A)$ compared with expectations from simulations for mixed composition discussed above, light $(p + \alpha)$, and heavy $(A > 4)$ composition. The comparison of the complete distribution for the X_{max} mass at 4 PeV is shown in the right panel of Fig. 5 as data points with errors. This also shows the expected distributions for a mixed composition (line), light (dashes), and heavy (dots). Although this is not the method of choice for the most accurate composition determination, these data alone seem to exclude a pure Fe composition over all of this energy range. Unlike other methods which use the distribution of

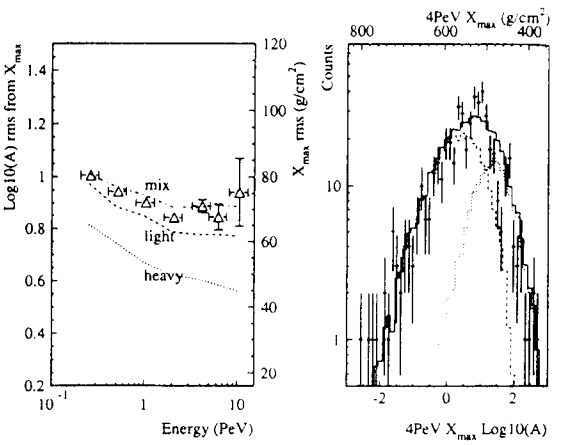

Fig. 5. (Left) X_{max} mass distribution r.m.s. widths compared with simulations across all measured energy bins. The right-hand axis is labelled with the equivalent r.m.s. width in X_{max}. (Right) Detailed X_{max} mass distribution at 4 PeV compared with simulations discussed in the text. The top axis is labelled with the corresponding values of X_{max} using Eq. (A.2).

Cherenkov light at ground level, the mass determination of DICE does not produce a long tail for $\log_{10}(A)_x$ in the negative region. This is because DICE intrinsically rejects all showers with an apparent X_{max} deeper than ~ 750 g/cm^2 by geometry. This provides some truncation of the distribution produced of the mass function which is incorporated in the simulation.

With distributions such as shown in the right-hand panel of Fig. 5 the mass resolution of the DICE $\log_{10}(A)_x$ measurements can be estimated. These are shown in Fig. 6 for incident protons and iron nuclei as a function of particle energy. The ordinate shows the r.m.s. resolution of the DICE experiment for the $\log_{10}(A)_x$ of a single event. The improvement in the resolution with increasing energy arises from a combination of larger light yield and an improving X_{max} resolution with the better event geometry in DICE of deeper showers. The mass resolution of proton showers at energies above a few PeV is close to the intrinsic limit for a mass based on X_{max} determination. Even if the depth of shower maximum and the shower energy is known perfectly, the mass resolution in $\log_{10}(A)$ for protons is limited to $\sigma \sim 0.8$ because of intrinsic fluctuations in the shower development. The mass resolution for iron showers is significantly better than for protons because the in-

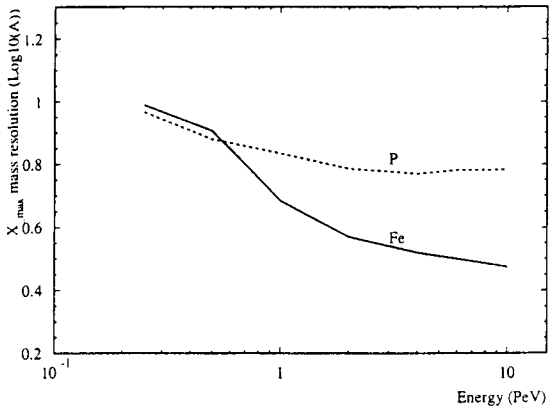

Fig. 6. The r.m.s. resolution derived from simulations for single events for $\log_{10}(A)$ derived from the measurement of X_{max} by DICE. The dashed curve is for proton events, the solid line for iron nuclei.

particles. The simulation can then be used to make corrections to the samples produced by estimating the amount of 'leakage' of heavier events into the (proton + α) sample. The results of an analysis on these data which uses a cut to extract the events where $\log_{10}(A) \leq 0$ are shown in the lower panel of Fig. 7 for the DICE X_{max} results. Similar analyses have not been made for the ground size distributions because simplifications in the fluctuations for these data make this method unreliable. The errors on the (p + α) fraction are based on simple counting statistics, the uncertainty is larger for this analysis method because fewer events pass the data cuts. There is a tendency of these results to a higher fraction of (p + α) at the higher energies although they are also consistent with constant composition across this re-

trinsic fluctuations of showers from these nuclei are significantly smaller. It is sobering to realize that iron is separated by only $\sim 2\sigma$ from an incoming proton signal for single events.

5. Composition determination

Using these methods a mass estimate for each event can be derived from (i) X_{max}, (ii) muon and electron size, and (iii) a simple linear combination of the two, called $\log_{10}(A)_c$. This last method has the advantage of somewhat increased resolution because the methods are to some extent independent. Each event is assigned values for $\log_{10}(A)_x$, $\log_{10}(A)_g$, and $\log_{10}(A)_c$ and collected in bins of energy. The results for the mean $\log_{10}(A)$ values versus energy are shown as the upper panel in Fig. 7. The mass error is based on statistics and the energy error is the estimate of the systematic error in the energy scale of the fits discussed earlier. All of the mass estimates show variations with energy across the knee region. These data are tabulated in Appendix B.

Another method for determining composition has been used (see e.g. Watson [27]) which attempts to separate a sample of almost pure proton + α events by applying a simple cut to the mass distribution, such as shown in Fig. 5, which excludes heavy

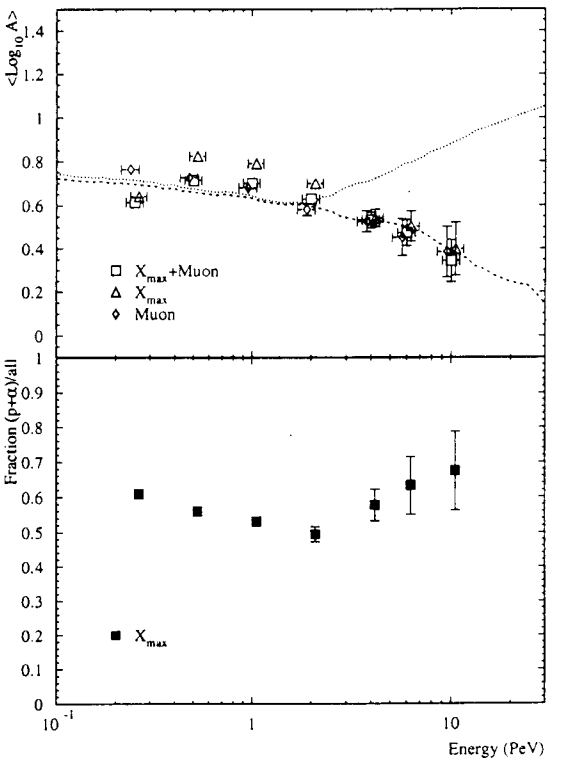

Fig. 7. (Top) Results for mean $\log_{10}(A)$ measurements from this work versus energy, the model curves are discussed in the text. (Bottom) Derived fraction of (p + α)/all for the X_{max} mass determination.

gion. The values of the $(p + \alpha)$ fraction are tabulated in Appendix B.

6. Discussion

By using several parameters measured for each shower a mass estimate for each incoming primary particle can be extracted which shows remarkable consistency between values derived from X_{max} and from the μ/e method. The direct observation of the expected shape and absolute normalization of showers in this energy range (Fig. 3) is a crucial test for the absence of systematic errors in the methods of mass estimation. The widths of the distributions shown in Fig. 5 are consistent with the results shown Fig. 7. These results essentially exclude an all-iron composition at 10 PeV, this conclusion was reached by an earlier analysis of DICE. The results suggest a tendency to lighter composition at high energies, although those from the ratio method are consistent with constant composition. A composite mean $\log_{10}(A)_c$ using both estimates shows a decreasing mass across the energy range of the knee region. For comparison, two models of possible cosmic-ray mass variation near the knee are plotted in Fig. 7. The dotted curve is the model given by Swordy 1995, where a source spectrum $\propto E^{-3}$ is introduced above the knee region and the energy dependent escape from the Galaxy is assumed to reach a plateau near the knee region. This model provides an increase in mass across the knee of a size which is larger than for models based simply on particle rigidity. The lower dashed line, with which the data seem more consistent, is a model which has similar low energy behavior as the previous model but which introduces a proton source which compensates for the lost flux above the SNR acceleration cutoff rigidity, assumed here to be 10^{15} V. This is similar to the suggestion of Protheroe and Szabo 1992 [28] where an extragalactic component of particles produced by AGNs provide the cosmic rays at high energy. These data seem more consistent with this latter model, where cosmic rays become progressively lighter across the knee region. However, they do not exclude the possibility that the composition is more or less constant across this energy range. A sudden change in composition to becoming predominantly iron nuclei ($\log_{10}(A) = 1.75$) seems strongly excluded. The variations in the energy spectrum of Fig. 1 near 8 PeV and the irregularity in the behavior of $\log_{10}(A)$ near 4 PeV shown in Fig. 5 lend some support to the single source model of the knee region discussed by Erlykin and Wolfendale [29]. However, Fig. 7 does not show the expected increase in $\langle \log_{10}(A) \rangle$ of ~ 0.4 across the knee region predicted by this model.

Contrary to conventional wisdom these results do not support a simple 'rigidity steepening' which would lead to a steady increase in mass across the knee region. If the cosmic-ray abundances below the knee are provided with a simple steepening from a spectrum of $E^{-2.75}$ to $E^{-3.0}$ and a composition below the knee is similar to that described by Swordy [22], the size of the effect should be an increase of ~ 0.2 in the mean value of $\log_{10}(A)$ across the knee. The combination of experimental measurements discussed here have the sensitivity to detect an increase of this order if it were present.

The mass resolution of these methods is poor when compared with direct techniques. The 1σ (r.m.s.) widths of the resolution in $\log_{10}(A)$ for nuclei have typical size $\sigma \sim 0.8$. Hence protons which fluctuate upward by $\sim 2\sigma$ can be misidentified as iron nuclei. In this measurement environment any methods which produce a lower intrinsic systematic error in the technique are extremely valuable. The philosophy behind DICE is to try to reduce these types of error by decreasing the reliance on Monte Carlo simulations of airshowers in the interpretation of the data. The method of directly measuring X_{max} from geometry avoids steps associated with inferences about the location of X_{max} from other variables such as the density distribution of particles at ground level which are interpreted with simulations. Only the probability of Cherenkov emission as a function of angle with the shower axis is needed to estimate X_{max} with DICE. This is relatively insensitive to the details of the simulation.

The use of X_{max} as a variable for composition determination is desirable for other reasons. The mass estimate derived from this variable is less sensitive to uncertainties in the characterization of shower parameters. To explore the sensitivity of the results to the analysis procedures a simple test can be made on the data set by exploring the trend of the derived masses for different values of the analysi

parameters. The results of this test are shown in Fig. 8. Here the upper panel shows two lines which are the trend of the data, as shown in Fig. 7, under two assumptions for the value of the elongation rate, X_m in Eq. (A.2). The solid line uses $X_m = 80$ g/cm^2 in the analysis, the dashed line uses $X_m = 75$ g/cm^2. The smaller elongation rate increases the apparent lightening of composition by an amount of ~ 0.1 in $\langle \log_{10}(A) \rangle$, giving an estimate of the systematic uncertainties in the analysis of the DICE X_{max} data. The lower panel shows a similar test of the μ/e mass derived from ground particle densities. Here the solid line represents the superposition model where $\alpha = 0.87$ in Eq. (3), the dashed line is an analysis where $\alpha = 0.82$. This mass estimate is clearly sensitive to the precise value of α used since this change makes $\langle \log_{10}(A) \rangle$ apparently *increase* by an amount ~ 0.2 across this energy region. The systematic error in the μ/e mass is therefore large since simulations typically give values of α in the range ~ 0.8–0.9. The above analyses illustrate a crucial property of multiparameter measurements in this type of work: the requirement for consistency from a variety of apparently redundant measurements can directly assess the validity of the result. In the case discussed here the mean mass estimates from the different techniques must agree since these are the same events, consequently an analysis where $X_m = 75$ g/cm^2 and $\alpha = 0.82$ is excluded by this consistency check.

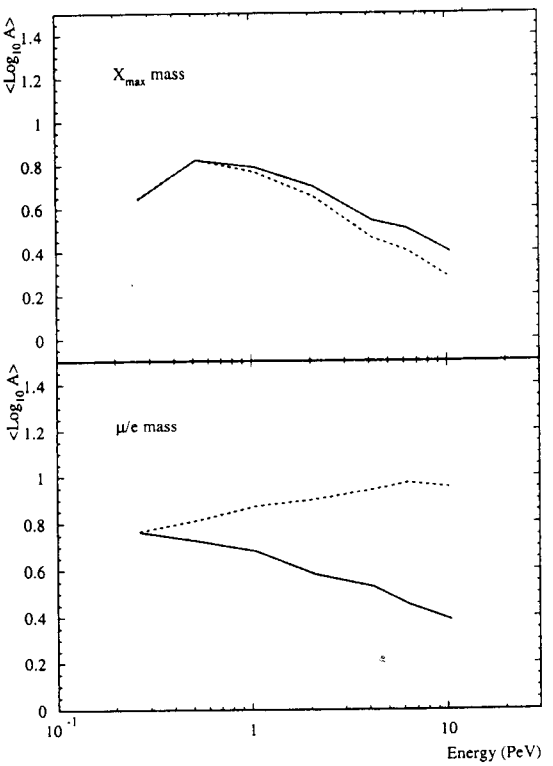

Fig. 8. (Top) The sensitivity of the X_{max} mass measurement to the elongation rate assumed. The solid line shows the trend of the data with the rate 80 g/cm^2 as used in this analysis, the dashed line shows the trend of an analysis using 75 g/cm^2. (Bottom) The sensitivity of the μ/e mass measurement to the analysis parameters. The solid line shows the trend of the data analyzed with a superposition model where $N_\mu \propto E^{0.87}$ as used here. The dashed line shows the trend produced if the analysis assumes $N_\mu \propto E^{0.82}$.

The instrumentation of ground-based cosmic-ray air shower detectors have improved significantly over the past decade or so. The statistical quality of these measurements has improved to the point where the intrinsic fluctuations in the shower developments are becoming the limiting factor in the determination of primary composition. The new challenge emerging in the derivation of composition from measurements of airshowers is the identification and quantification of systematic errors in aspects of the measurements themselves or in the simulations used for analysis. By making use of multiparameter measurements of the same showers we can directly explore our level of understanding of these issues and provide a reliable determination of cosmic-ray composition in this energy region. The results presented here are an attempt to take some initial steps in this direction.

Acknowledgements

The authors gratefully acknowledge the assistance of the HiRes collaboration and Ryan Lawrence. We thank M. Cassiday for technical support and the commander and staff of the US Army Dugway Proving Grounds for assistance. Thanks are due to our colleagues who collected much of these data, these include Kevin Boothby, Mark Chantell, Curtis Larsen, Kevin Green, and the entire CASA-MIA group. We are also grateful to useful discussions with Clem Pryke. This work is supported through the Block Fund at the University of Chicago and institu-

tional support and by the National Science Foundation Grant PHY 9514193 at the University of Utah.

Appendix A. Fitting functions

A.1. Cherenkov light distribution function

This function which is used to fit the Cherenkov light sizes at the DICE detectors is derived from simulations using CORSIKA 4.5 with VENUS [19] and is valid for shower core distances larger than 75 m from each DICE cluster. It depends on particle energy, mass and event geometry as follows:

$$Ch = C_0 E(\mathrm{PeV})^{\gamma} A^{-\epsilon} \mathrm{e}^{-\beta r(m)}, \qquad (A.1)$$

where

$C_0 = 1.89 \times 10^6$,

$\gamma = 1.144 + 0.0905 \times \log_{10}(A)$,

$\beta = 0.0161 \times \big(1 - 0.128 \times \log_{10}(A) + 0.124 \times \log_{10}(E(\mathrm{PeV})) \times (1 + 0.322 \times \log_{10}(A))\big)$,

$\epsilon = 0.186$.

Here Ch is the number of Cherenkov photons collected in the effective area ($3.75\mathrm{m}^2$) of a DICE detector. The total energy of the shower in PeV is E(PeV), A is the mass of the incident particle, and $r(m)$ is the perpendicular distance to the shower core from the DICE detector. Note the amount of light varies almost linearly with energy (γ) since the Cherenkov size is close to a calorimeteric measurement of the shower energy because nearly all of the particles produced in the shower give Cherenkov light. The light intensity also decreases with increasing mass for the same total energy (ϵ). The light intensity falls with distance from the shower core, for low mass particles near 1 PeV the light intensity falls with a scale distance of ~ 62 m ($1/\beta$). For iron nuclei at similar energies the scale distance is ~ 80 m.

A.2. $X_{\max}$ fitting function

The following equation is the fitting function u for the primary mass and energy dependence for location of $X_{\max}$:

$$X_{\max} = X_0 + X_m \times (\log_{10}(E) - \log_{10}(A)), \qquad (A$$

where

$X_0 = 560\,\mathrm{g/cm}^2$,

$X_m = 80\,\mathrm{g/cm}^2$,

where $X_{\max}$ is the location of shower maximum and A are the incident particle energy in PeV particle mass (in nuclear mass units), respectivel

A.3. Gaisser shower size function

The function used for the average shower de opment is adapted from Gaisser [26] to calculate expected electron size at ground level, X_0, fc shower of total energy E with a maximum at a de $X_{\max}$,

$$N_e(X_0) = A_e \times E(\mathrm{PeV}) \times p/(p+1) \times e^{p}\big(X_0/(X_{\max} - \lambda)\big)^{(p+1)} \mathrm{e}^{-X_0/\lambda}. \qquad (A$$

Here $A_e = 6.02 \times 10^5$ is a constant, E(PeV the shower energy in PeV, $X_0 = 860\ \mathrm{g/cm}^2$ is average detector atmospheric depth, $p = X_{\max}/\lambda$ and $\lambda = 70\ \mathrm{g/cm}^2$ is the hadronic interaction len This assumes simple scaling in the Gaisser funct i.e. $S_0 = 0.045$ and $\epsilon = 0.074$ GeV. The lower r panel of Fig. 3 shows the effect of the sca

Table 2
Table of $X_{\max}$ versus energy from DICE.

Energy bin (PeV)	Median energy (PeV) (PeV)	$\langle X_{\max} \rangle$ ($\mathrm{g/cm}^2$)
0.2–0.4	0.26 ± 0.05	470.7 ± 0.6
0.4–0.7	0.50 ± 0.10	476.3 ± 0.8
0.7–1.5	0.91 ± 0.18	497.7 ± 1.0
1.5–3.0	1.92 ± 0.38	529.6 ± 1.6
3.0–5.0	3.66 ± 0.73	562.8 ± 3.3
5.0–8.0	6.03 ± 1.21	587.4 ± 5.5
8.0–15.0	10.09 ± 2.02	610.3 ± 10.0

Table 3
Table of mass estimates from DICE, ground sizes from CASA/MIA and from a combination of the two methods. Also given is the result of the $(p + \alpha)$/all fraction estimate, discussed in the text.

Energy (PeV)	Combined $\langle \log_{10}(A) \rangle$	X_{max} $\langle \log_{10}(A) \rangle$	μ/e $\langle \log_{10}(A) \rangle$	$(p + \alpha)$/all
0.2	0.61 ± 0.01	0.64 ± 0.01	0.76 ± 0.01	0.609 ± 0.011
0.5	0.71 ± 0.01	0.82 ± 0.01	0.73 ± 0.02	0.560 ± 0.012
1.0	0.70 ± 0.01	0.79 ± 0.01	0.68 ± 0.02	0.531 ± 0.014
2.0	0.63 ± 0.02	0.70 ± 0.02	0.58 ± 0.03	0.494 ± 0.022
4.0	0.53 ± 0.04	0.54 ± 0.04	0.53 ± 0.05	0.577 ± 0.045
6.0	0.47 ± 0.06	0.51 ± 0.07	0.45 ± 0.09	0.633 ± 0.082
10.0	0.34 ± 0.10	0.40 ± 0.12	0.39 ± 0.12	0.674 ± 0.112

violation suggested by Gaisser [26] as a dashed curve.

Appendix B. Tabulated results

This appendix contains Tables 2, 3 and 4 of the results of this investigation.

Table 4
The all particle fluxes of cosmic rays from DICE

Total particle energy (GeV)	Flux (m^2 sr s GeV)$^{-1}$	Flux error ($\pm$(m^2 sr s GeV)$^{-1}$)
0.355×10^6	0.361×10^{-10}	0.50×10^{-12}
0.447×10^6	0.208×10^{-10}	0.30×10^{-12}
0.562×10^6	0.115×10^{-10}	0.18×10^{-12}
0.708×10^6	0.619×10^{-11}	0.11×10^{-12}
0.891×10^6	0.322×10^{-11}	0.65×10^{-13}
0.112×10^7	0.167×10^{-11}	0.39×10^{-13}
0.141×10^7	0.906×10^{-12}	0.24×10^{-13}
0.178×10^7	0.496×10^{-12}	0.15×10^{-13}
0.224×10^7	0.263×10^{-12}	0.96×10^{-14}
0.282×10^7	0.142×10^{-12}	0.61×10^{-14}
0.355×10^7	0.734×10^{-13}	0.38×10^{-14}
0.447×10^7	0.333×10^{-13}	0.23×10^{-14}
0.562×10^7	0.163×10^{-13}	0.14×10^{-14}
0.708×10^7	0.711×10^{-14}	0.82×10^{-15}
0.891×10^7	0.557×10^{-14}	0.64×10^{-15}
0.112×10^8	0.207×10^{-14}	0.35×10^{-15}
0.141×10^8	0.999×10^{-15}	0.21×10^{-15}
0.178×10^8	0.430×10^{-15}	0.12×10^{-15}
0.224×10^8	0.113×10^{-15}	0.57×10^{-16}
0.282×10^8	0.112×10^{-15}	0.50×10^{-16}

Appendix C. Details of the muon mass function

As has been mentioned in the main text the mass derived from the muon size, Eq. (3), is susceptible to variations introduced by fluctuations from the location of shower maximum. Although these are not as large as associated with the electron size shown in Fig. 3, they produce poor resolution in the muon mass function unless corrected. A quantitative measure of this effect is shown in Fig. 9

The normalized muon mass size $(\log_{10}(N_\mu/E(\text{PeV}))$ is derived from the MIA muon size and the DICE Cherenkov energy, E(PeV). This size is clearly

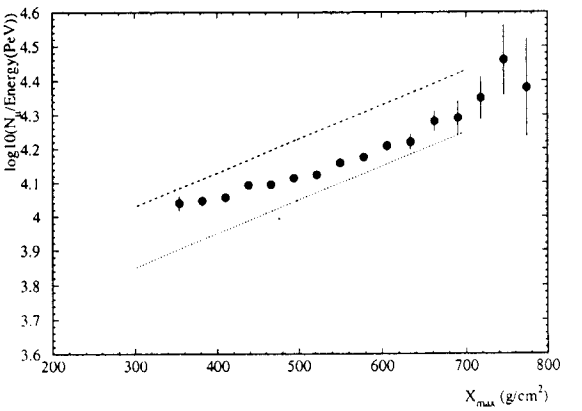

Fig. 9. The variation of the normalized log10(muon size/energy) with depth of shower maximum (X_{max}) around 1 PeV is shown as the filled symbols. There is a clear correlation between the depth of shower maximum and the normalized muon size. The lower dotted line is a simulation of this effect for masses $A \leq 4$, the upper dashed line is a simulation for $A > 4$ using the same composition discussed in the text.

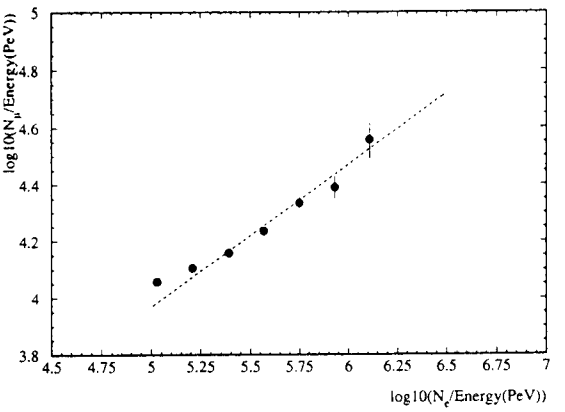

Fig. 10. The variation of the normalized log10(muon size/energy) with normalized log10(electron size/energy) near 1 PeV. The line is a fit with a slope of 0.5, this is discussed further in the text.

correlated with X_{max} depth at energies near 1 PeV as shown. This is a weaker version of the effect shown for electrons in Fig. 3. It presumably arises from more muons either decaying or reaching the end of the range for the showers with maxima higher from the ground. Although at a fixed X_{max} the muon mass function will perform as desired, the presence of fluctuations smears the possible mass resolution because of this effect. Indeed as the relationship between the simulation curves (dashed lines) on Fig. 9 and the measured data show, in general as the shower penetrates more deeply the muon content appears more 'proton-like' as expected. To produce a more accurate mass function a variable must be introduced to offset the effect of shower depth shown in the figure. Since electron size is closely correlated with X_{max}, as shown in Fig. 3, this can be used to make a correction and provide a mass function from the ground sizes which is completely independent from the X_{max} measurement of DICE and therefore provide a separate mass estimate for each shower.

Fig. 9 shows the basis for this correction. For showers near 1 PeV the average muon size, normalized by the Cherenkov energy, is plotted against the normalized electron size. The variations in these sizes come predominantly from the fluctuations in X_{max} between showers. Fig. 9 represents on average how the muon size changes with electron size due to these fluctuations. The dashed line is a linear fit to these data with a slope of 0.5. The electron size correction to the muon size mass measure is therefore of the form

$$\delta(e_g) = 0.5 \times \left(e_g - 1.14 \times \log_{10} E(\mathrm{PeV})\right), \tag{C.1}$$

where $e_g = \log_{10}(N_{ec}/N_{e0})$ as before, and where the second term corrects for the average electron size increase with energy. This effectively provides a correction for the muon size growth with X_{max} shown in Fig. 10.

References

[1] G.V. Kulikov et al., JETP 35 (1958) 635.
[2] J.H. Buckley et al., Astron. & Astrophys. 329 (1998) 639.
[3] L.O'C. Drury, F.A. Aharonian, H.J. Völk, Astron. & Astrophys. 287 (1994) 959.
[4] J.A. Esposito et al., Astrophys. J. 461 (1996) 820.
[5] Brazier et al., Mon. Not. R. Astron. Soc. 281 (1996) 1033.
[6] M. Koyama et al., Nature 378 (1995) 255.
[7] M. Keohane et al., Astrophys. J. 484 (1997) 350.
[8] S.P. Reynolds, Astrophys. J. 459 (1996) L13.
[9] R. Schlickeiser, Astrophys. J. Supp. 90 (1994) 929.
[10] J.A. Simpson, M. Garcia-Munoz, Space Sci. Rev. 46 (1988) 205–224.
[11] J.A. Simpson, J.J. Connell, Astrophys. J. 497 (1998) L85.
[12] A. Borione et al., Nucl. Instrum. Methods A 346 (1994) 329.
[13] K. Boothby et al., Proc. 24th Int. Cosmic Ray Conference. Rome, Vol. 2 (1995) p. 697.
[14] K. Boothby et al., Nucl. Phys. B (Proc. Suppl.) 52B (19??) 166.
[15] K. Greisen, Ann. Rev. Nucl. Sci. 10 (1960) 63.
[16] K. Kamata, Nishimura, J. Prog. Theor. Phys. Supp. 6 (1958) 93.
[17] T. McKay, PhD Thesis (University of Chicago, 1992).
[18] K. Boothby et al., Astrophys. J. Lett. 491 (1997) L35–L38.
[19] D. Heck et al., CORSIKA: A Monte Carlo program to Simulate Extensive Air Showers, Forschungszentrum Karlsruhe Report FZKA 6019 (1998).
[20] J. Cortina et al., Proc. 25th Int. Cosmic Ray Conference. Durban, Vol. 4 (1997) p. 69.
[21] O.A. Gress et al., Proc. 25th Int. Cosmic Ray Conference. Durban, Vol. 4 (1997) 129.
[22] S.P. Swordy, Proc. 23rd Int. Cosmic-Ray Conf. (Calgary). Invited and Rapporteur (1993) p. 243.
[23] Amenomori et al., Astrophys. J. 461 (1996) 408.
[24] M.A.K. Glasmacher et al., Astropart. Phys. 10 (1999) 291.
[25] M. Nagano et al., J. Phys. G 10 (1984) 1295.
[26] T.K. Gaisser, Cosmic Rays and Particle Physics, (Cambridge Univ. Press, Cambridge, 1990) p. 239.
[27] A.A. Watson, Rapporteur talk, Proc. 25th Int. Cosmic-Ray Conf., Durban (1997).
[28] R.J. Protheroe, A.P. Szabo, Phys. Rev. Lett. 69 (1992) 2885.
[29] A.D. Erlykin, A.W. Wolfendale, Astropart. Phys. 265 (1998).